


## Research Article

# Variation of the winter mid-latitude Westerlies in the Northern Hemisphere during the Holocene revealed by aeolian deposits in the southern Tibetan Plateau

Fuyuan Gao<sup>a,b\*</sup> , Junhuai Yang<sup>c</sup>, Shuyuan Wang<sup>c</sup>, Youjun Wang<sup>d</sup>, Kaiming Li<sup>a</sup>, Fei Wang<sup>c</sup>, Zhiyong Ling<sup>c,e</sup> and Dunsheng Xia<sup>c\*</sup>

<sup>a</sup>College of Geography and Environmental Engineering, Lanzhou City University, Lanzhou, 730070, China; <sup>b</sup>School of Geographic Sciences, East China Normal University, Shanghai, 200241, China; <sup>c</sup>Key Laboratory of Western China's Environmental Systems (Ministry of Education), College of Earth and Environmental Sciences, Lanzhou University, Lanzhou, 730000, China; <sup>d</sup>College of Tourism and Environmental Resource, Zaozhuang University, Zaozhuang, 277160, China and <sup>e</sup>Key Laboratory of Comprehensive and Highly Efficient Utilization of Salt Lake Resources, Qinghai Institute of Salt Lakes, Chinese Academy of Sciences, Xining, 810008, China

### Abstract

The mid-latitude Westerlies (MLW) are one of the most important atmospheric circulation systems in the Northern Hemisphere, exerting a huge influence on the climate of the region downwind, and thus on vegetation, water resources, and human wellbeing. However, the seasonal variation of the MLW during the Holocene is not yet been fully understood, especially when its contribution is the most important. Here, we used end-member (EM) modeling analysis of the grain-size distributions of a high-altitude aeolian sedimentary sequence (4452 m a.s.l.) from the Yarlung Zangbo River valley in the southern Tibetan Plateau to reveal variations in the winter MLW during the Holocene. Analysis of seasonal differences in modern atmospheric circulation suggests that the southern Tibetan Plateau was heavily influenced by the mid-latitude Westerlies at the 400, 500, and 600 hPa levels in winter, while it was seldom influenced at these levels in summer. Four grain-size end-members are identified, representing distinct aerodynamic environments, of which EM1 (modal grain size 8.1  $\mu\text{m}$ ) can be used as a proxy of the winter MLW. A reconstruction of the variation of the winter MLW during the Holocene based on EM1 revealed that a weaker winter MLW occurred during the Early to Middle Holocene, and a stronger winter MLW during the Middle to Late Holocene. Overall, we suggest that this change in the winter MLW was closely related to the insolation/temperature/pressure gradient between low and high latitudes in the Northern Hemisphere.

**Keywords:** Holocene, Climate change, Mid-latitude Westerlies, End-member analysis, Grain size, Aeolian sedimentary sequence, Yarlung Zangbo River

(Received 2 June 2021; accepted 10 October 2021)

### INTRODUCTION

As a major atmospheric circulation system, the mid-latitude Westerlies (MLW) played an important role in climatic and environmental changes in the Northern Hemisphere, as well as in the evolution of civilization, especially in arid Central Asia and parts of the Tibetan Plateau (e.g., Chen et al., 2016, 2019; Ling et al., 2020). The MLW transport water vapor from the water bodies upwind (i.e., the Mediterranean Sea, Caspian Sea, and Black Sea), causing variations in modern precipitation (as well as during the Holocene) in arid Central Asia (An et al., 2012; Wang et al., 2013; Chen et al., 2016; Song et al., 2021) and the southern Tibetan Plateau (Tian et al., 2005; Hou et al., 2017; Sun et al.,

2020; Kumar et al., 2021). Numerous studies have tried to extract information about the intensity of the MLW from sedimentary grain-size distributions, because the MLW transports fine-grained particles to the regions downwind. The results of the grain-size analysis of aeolian deposits in the regions dominated by the MLW indicate that the fine-grained fraction (2–10  $\mu\text{m}$ ) is an index of the intensity of the MLW (Sun, 2002; Vandenberghe, 2013; Jia et al., 2018, Wang et al., 2019; Duan et al., 2020).

End members (EMs) with modal grain sizes of 11  $\mu\text{m}$  (EM2 in the LJW10 section) and 5  $\mu\text{m}$  (EM2 in the TLD16 section) were identified in loess deposits from the Tien Shan Mountains, in eastern arid Central Asia (Jia et al., 2018, Wang et al., 2019), which suggests that these fractions were transported by the MLW (in upper-level long-term suspension). Therefore, variations in the sedimentary contribution of the end-members was used to reconstruct past variations in the MLW, and on this basis weaker MLW occurred during the Early to Middle Holocene and stronger MLW during the Middle to Late Holocene. Although both of these studies revealed the trend of

\*Corresponding authors. email addresses: <gaofy1014@126.com>; <dsxia@lzu.edu.cn>

Cite this article: Gao F, Yang J, Wang S, Wang Y, Li K, Wang F, Ling Z, Xia D (2022). Variation of the winter mid-latitude Westerlies in the Northern Hemisphere during the Holocene revealed by aeolian deposits in the southern Tibetan Plateau. *Quaternary Research* 107, 104–112. <https://doi.org/10.1017/qua.2021.65>

variation of the MLW during the Holocene, on an annually averaged basis, the seasonal variations of the MLW remain unclear, especially in winter. Modern meteorological observations and paleoclimatic records have suggested that variation of the MLW in winter makes an important contribution to precipitation in arid Central Asia (Wang et al., 2013; Long et al., 2017) and the southern Tibetan Plateau (Tian et al., 2005; Schiemann et al., 2009; Yang et al., 2021).

To address the issue of seasonal variations in the MLW, we studied a high-altitude aeolian sedimentary sequence from the Yarlung Zangbo River valley in the southern Tibetan Plateau, at an elevation >4000 m above sea level (a.s.l.), and then analyzed the modern atmospheric circulation in this region. Our aim was to determine the trend of variation of the winter MLW in the Northern Hemisphere during the Holocene. We extracted a signal of the winter MLW using end-member modeling analysis of the grain-size distributions of the studied sedimentary sequence, and combined with the published chronological framework for the section, we reconstructed the evolution of the winter MLW in the Northern Hemisphere during the Holocene. Finally, we discussed the possible driving mechanism behind the observed changes.

## MATERIALS AND METHODS

### Geographical setting

The Yarlung Zangbo River flows from west to east across most of the southern Tibetan Plateau (Fig. 1). Aeolian deposits are mainly distributed in the wide river valley at an average altitude of nearly 4000 m, including the Maquanhe wide valley, Shigatse wide valley, Shannan wide valley, and Mainling wide valley, from west to east, lying mainly within the area of 29.25–29.75°N and 88–92°E (Ling et al., 2019; Yang et al., 2020a). There is almost no aeolian accumulation in the narrow valleys due to the lack of sediment supply and the strong winds. The mean annual temperature in this region ranges from 1.5–8.8°C, and the mean annual precipitation ranges from 131.6–676.7 mm (Shen et al., 2012). Aeolian activity occurs mainly in the winter and spring, and the mean annual near-surface wind speed ranges from 1.6–3.3 m/s (Yang et al., 2020b).

### Studied aeolian section

The Sagaxi (SGX) section (29°19′20.33″N; 85°10′3.93″E, 4452 m a.s.l.) is located in the upper reaches of Yarlung Zangbo River in the southern Tibetan Plateau (Fig. 1). The section is 360 cm thick, and the following stratigraphic units can be defined: 0–100 cm, compact light-yellow loess with calcareous cement and relatively fine particles, the uppermost 10 cm contains a small quantity of plant roots; 100–200 cm, loose gray-brown sandy loess with abundant white calcium mycelium and coarser particles; 200–360 cm, relatively loose gray-brown sandy loess, with two gravel layers at 290–300 cm and 310–315 cm (Fig. 2b). We collected 144 samples at a 2.5-cm interval for measurements of grain size and geochemical and magnetic proxies. Eleven optically stimulated luminescence samples were also collected to establish a robust chronology, using the single-aliquot regeneration method, which is reported in Yang et al. (2021) (Fig. 2a).

### Grain-size analysis

We used the pretreatment methods of Lu and An (1998) for the grain-size samples. All samples of the SGX section were heated

with 10 mL of 30% H<sub>2</sub>O<sub>2</sub> and 10% HCl to remove organic matter and carbonate, respectively. To remove acid ions, the samples were suspended in deionized water for 12 hr. The samples were then dispersed by adding 10 ml of 0.05 mol/L (NaPO<sub>3</sub>)<sub>6</sub> and treating them with ultrasound for 10 min. Grain-size frequency distributions were made with a Malvern Mastersizer 2000 laser-diffraction particle size analyzer, which has a measurement range of 0.02–2000 μm. The Mie model was used to calculate the grain-size distributions, the default refractive index was 1.52, and the absorption coefficient was 0.1.

### Geochemical measurements

Measurements of the concentrations of geochemical elements were also performed on all samples. The samples were ground and passed through a 200-mesh sieve, and then 4 g of sediment were placed in a mold and boric acid added to the edge and base. The samples were then compressed into a disc with a diameter of 32 mm under 30 tons of pressure. Element concentrations were measured using a PW2403 X-Ray fluorescence (XRF) spectrometer.

The chemical index of alteration (CIA) has been widely used to evaluate the chemical weathering intensity of sediments, and is positively related to the weathering degree:

$$\text{CIA} = [\text{Al}_2\text{O}_3 / (\text{Al}_2\text{O}_3 + \text{CaO}^* + \text{Na}_2\text{O} + \text{K}_2\text{O})] \times 100$$

Oxides in the formula are expressed in molar ratios, and CaO\* refers only to CaO in silicates. Therefore, we calculated the CaO\* by removing the CaO contained in carbonates using the method of McLennan (1993), which assumes CaO/Na<sub>2</sub>O = 1 in silicates. If CaO/Na<sub>2</sub>O < 1, then CaO\* = CaO. However, if CaO/Na<sub>2</sub>O > 1, then CaO\* = Na<sub>2</sub>O. Changes in the weathering degree are closely related to climate change, with high CIA usually indicating a relatively warm and wet climate.

### Magnetic measurements

Air-dried samples were ground and packed in 2×2×2 cm<sup>3</sup> plastic boxes and used for measurements of low-frequency (470 Hz) and high-frequency (4700 Hz) magnetic susceptibility ( $\chi_{\text{lf}}$  and  $\chi_{\text{hf}}$ , respectively) using a Bartington MS2 magnetic susceptibility meter. The two parameters were used to calculate the frequency-dependence of magnetic susceptibility ( $\chi_{\text{fd}}$ ), which is defined as  $\chi_{\text{fd}} = \chi_{\text{lf}} - \chi_{\text{hf}}$ .

All of the above experiments were performed at the Key Laboratory of Western China's Environmental Systems (Ministry of Education), Lanzhou University, China.

## RESULTS

### End-member analysis

The numbers of EMs for the grain-size distributions were set from 1 to 10 and the end-member models are illustrated in Figures 3 and 4 (Fig. 4a shows that the grain-size distributions of the samples from the SGX section are polymodal). The fitting precision and the number of end members were determined by the coefficient of determination ( $R^2$ , Fig. 3a) and the angular deviation (Fig. 3b). Generally, a better-fitting precision is indicated by both a higher  $R^2$  and the lower angular deviation (Duan et al., 2020). When the number of EMs increases to four,  $R^2$  is almost

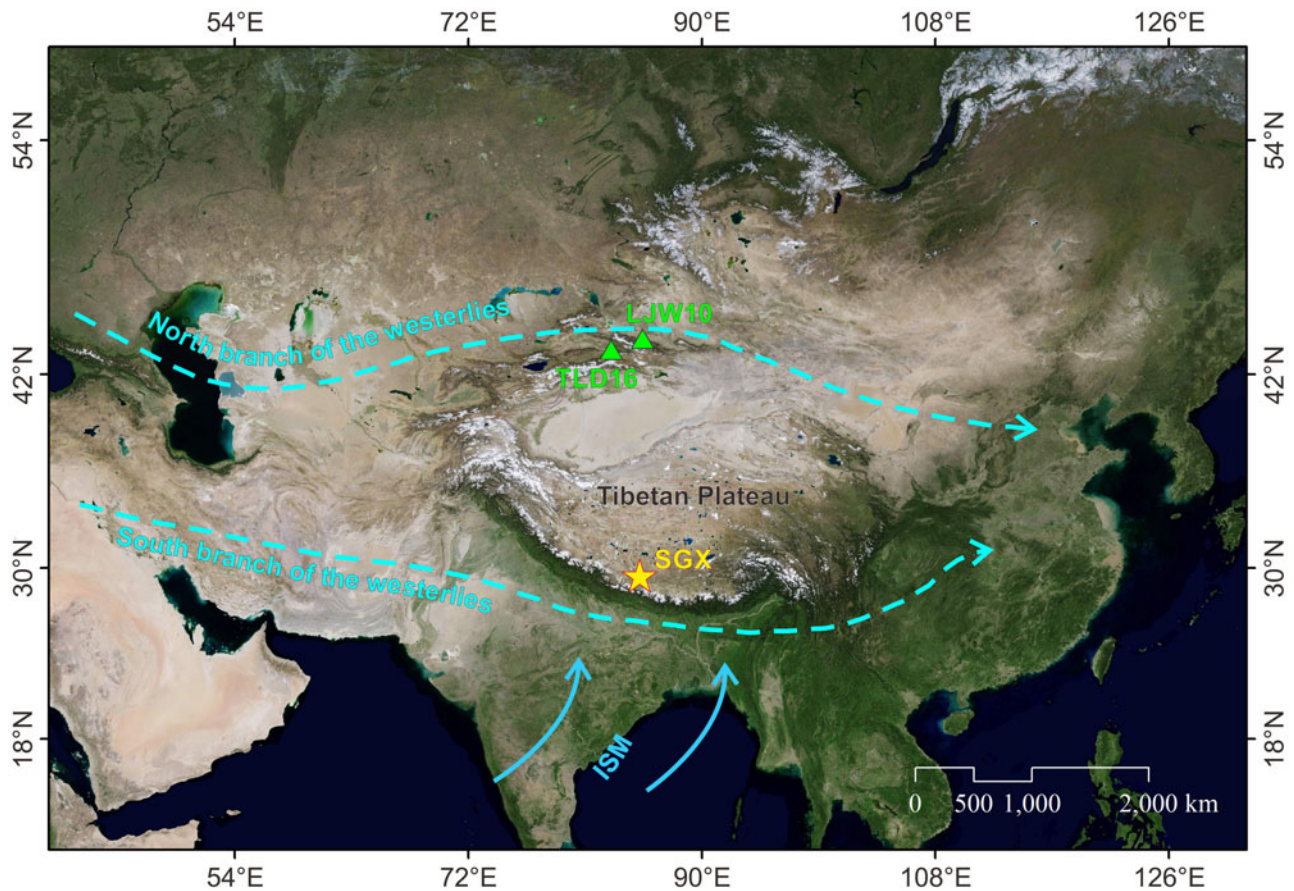


**Figure 1.** Location of the study area and the studied aeolian sedimentary sequence. The trajectories of the northern and southern branches of the mid-latitude Westerlies and the Indian summer monsoon are also shown. Abbreviations: ISM, Indian summer monsoon; SGX, Sagaxi section; TLD16, Talaide16 section; LJW10, Lujiaowan10 section.

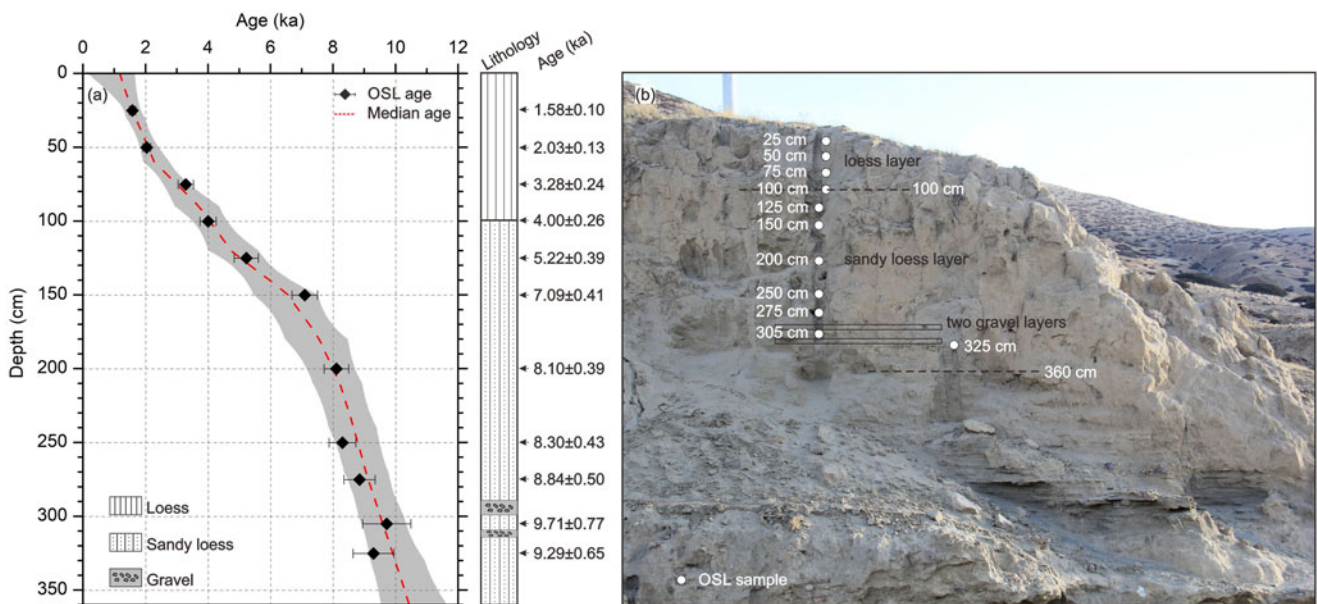


**Figure 2.** (a) Optically stimulated luminescence ages and (b) lithology for the SGX section. The chronological data are from Yang et al., 2021.

close to one and the angular deviation degree is  $<5$ , and at the same time, the correlation between the end members is relatively low ( $R^2 = 0.17$ ). Therefore, four EMs were identified for the SGX

section, with modal grain sizes of  $8.1 \mu\text{m}$  (EM1),  $66.4 \mu\text{m}$  (EM2),  $127.0 \mu\text{m}$  (EM3), and  $243.0 \mu\text{m}$  (EM4) (Fig. 4b). Combining the chronology of the SGX section with profiles of the EMs (Fig. 5)

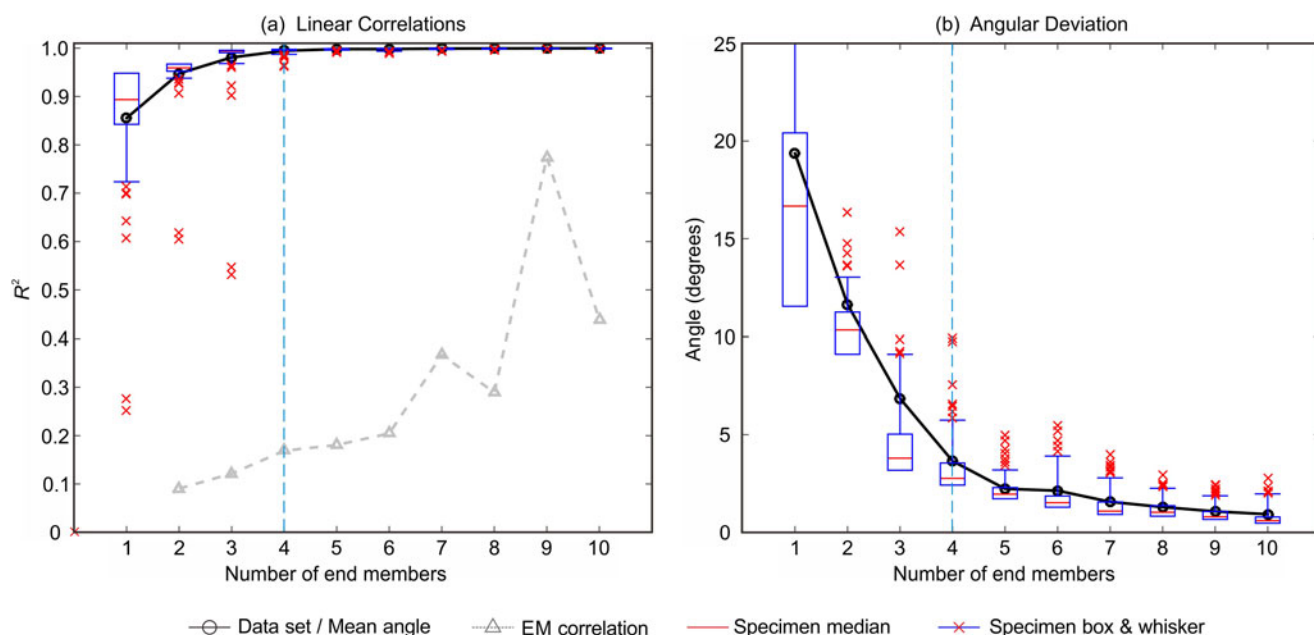


Figure 3. Linear correlations (a) and angular deviation (b) of the grain-size end members for the SGX section.

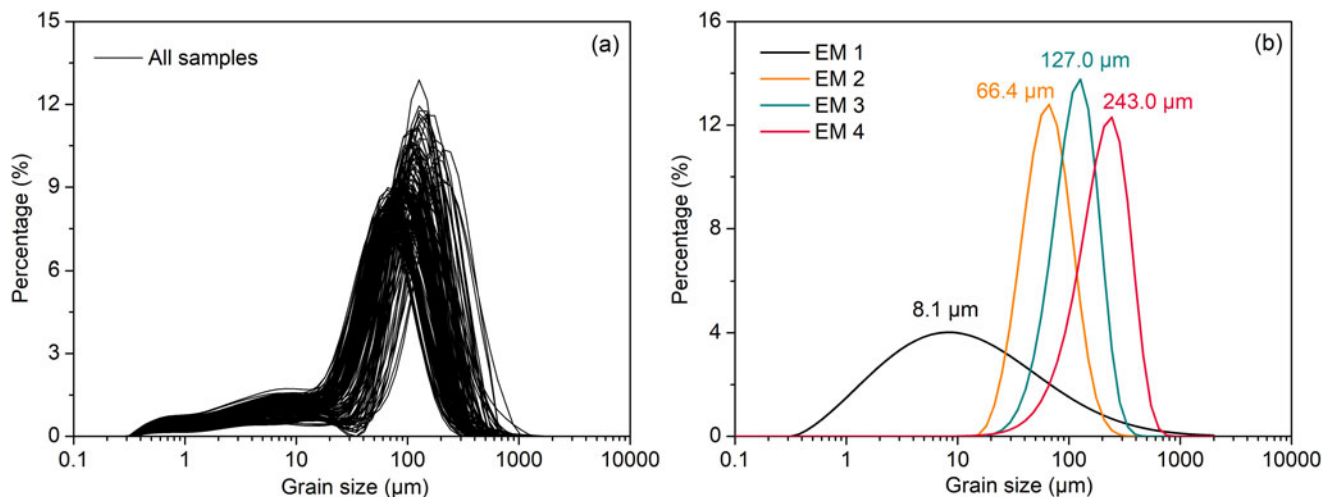


Figure 4. Grain-size frequency distributions for (a) all samples and (b) end members of the SGX section.

shows that the values of EM1 were lower before ca. 6 ka and that high values occurred during 6–1 ka. EM2 increased during 10.3–7.5 ka and high values occurred during 7.5–1 ka. EM3 gradually decreased, with fluctuations, during 10.3–1.0 ka. High values of EM4 occurred before 9 ka and lower values thereafter. Overall, the mean grain size gradually decreased during the Holocene (Fig. 5).

#### Seasonal differences in wind circulation

We used data from the National Center for Environmental Prediction/National Center for Atmospheric Research (NCEP/NCAR Reanalysis 1) for 1948–2016 to analyze seasonal changes in atmospheric circulation (Fig. 6). In summer, the southern Tibetan Plateau is influenced mainly by the Indian summer monsoon and rarely by the MLW, except at the 400 hPa level

(~7000 m) (Fig. 6a, c, e). In winter, the southern Tibetan Plateau is influenced solely by the MLW at the 400 hPa, 500 hPa, and 600 hPa levels (Fig. 6b, d, f). The Tien Shan Mountains, in eastern arid Central Asia, are dominated by the MLW at the 400 hPa, 500 hPa, and 600 hPa levels, in both summer and winter. In addition, the MLW in winter were stronger than in summer.

## DISCUSSION

### Paleoclimatic implications of EMs in the SGX section

As a continuous background supply of atmospheric dust (Vandenberghe, 2013), the 2–10  $\mu\text{m}$  grain-size fraction has been widely applied to reveal variations in the strength of the MLW (Sun, 2002; Jia et al., 2018; Wang et al., 2019; Duan et al.,

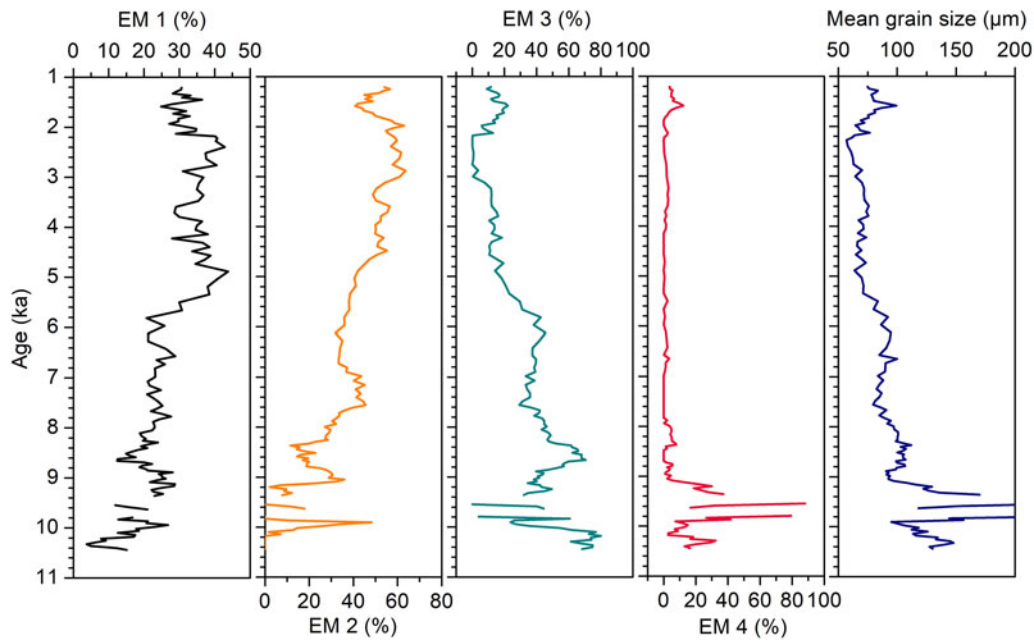


**Figure 5.** Time series of the four End members and the mean grain-size of the SGX section.

2020). Grain-size analysis of a loess section (LJW10, 43°58'29"N, 85°20'10"E) in the northern Tien Shan Mountains, in eastern arid Central Asia, indicated that EM1 (modal grain size 1.6 μm) was produced by pedogenesis, and that EM2 (modal grain size 11 μm) was transported by the Westerlies (Jia et al., 2018). End-member analysis of a loess section (TLD16, 43°20'99"N, 85°1'4.5"E) in the Yili valley, eastern arid Central Asia, indicated that EM1 (modal grain size 1 μm) was linked to pedogenesis, and that EM2 (modal grain size 5 μm) was closely related to the MLW (Wang et al., 2019). Another end-member analysis of a loess section (SCZ17, 43°37'2.34"N, 89°45'31.67"E), also in the northern Tien Shan Mountains, indicated that EM1 (modal grain size 5.3 μm) and EM2 (modal grain size 10.5 μm) were likely transported by the MLW and then deposited by rainout (Duan et al., 2020). Therefore, we infer that EM1 (modal grain size 8.1 μm, in this study) is closely linked to pedogenesis and the MLW.

The chemical index of alteration (CIA) of the samples from the SGX section are between 50 and 65. A plot of the CIA versus Na/K indicates the occurrence of only weak chemical weathering intensity in the SGX section (Fig. 7). The  $\chi_{fd}$  is a measure of the proportion of fine ferrimagnetic grains in magnetic mineral assemblages, and can be used as an indicator of the degree of pedogenic development of aeolian deposits (e.g., Chen et al., 2016; Gao et al., 2019). We compared the  $\chi_{fd}$  of loess-paleosol sequences from the Chinese Loess Plateau in northern China and the Tien Shan Mountains in northwestern China with the SGX section in this study. The results suggest that the  $\chi_{fd}$  values of the SGX section ( $<2 \times 10^{-5} \text{ m}^3/\text{kg}$ ) are significantly lower than those of paleosols from the Chinese Loess Plateau and the Tien Shan Mountains, and are similar to the values of loess from the Tien Shan Mountains, which reflect extremely weak weathering and pedogenesis (Fig. 8). Both the geochemical and magnetic evidence suggest that the contribution of pedogenesis to EM1 is very limited, and therefore that EM1 is likely dominated by the MLW. We also compared EM1 with geochemical element ratios (i.e., Na/K and Rb/Sr, Fig. 9f, g) which also reflect weathering

intensity in the region. The results show that high weathering intensity corresponds to low values of EM1 before 7.6 ka, which also indicates that EM1 is independent of variations in weathering and pedogenesis, and thus that it reflects the variation of the MLW.

The patterns of wind circulation show that in summer, the MLW at different altitudes have little influence on the study area, which is dominated by the Indian summer monsoon, especially at the 500 hPa and 600 hPa levels (Fig. 6a, c, e). Previous studies have indicated that the strength of the Indian summer monsoon, linked to Northern Hemisphere summer insolation, decreased gradually from the Early Holocene to the Late Holocene (Wang et al., 2005; Fleitmann et al., 2007). It is likely that the Indian summer monsoon is able to reach the study area at present, and thus it may also have influenced the area during the Holocene. In winter, the study area is dominated entirely by the MLW at the 400 hPa, 500 hPa, and 600 hPa levels (Fig. 6b, d, f); moreover, the MLW are much stronger in winter than in summer. This evidence suggests that the contribution of the MLW in winter to EM1 is much greater than in summer, and thus we propose that EM1 can be used as a proxy of the winter MLW. An enhanced winter MLW would transport more fine-grained particles to the study area. Such fine-grained particles (mainly  $<10 \mu\text{m}$ ) will be washed out of the atmosphere and deposited by precipitation (Pye, 1987, 1995), which would increase their proportion in aeolian deposits in the study area, resulting in an increase in EM1. Therefore, an increase in EM1 can be interpreted as an increase in winter MLW intensity.

EM2 (modal grain size 66.4 μm) is generally within the coarse-grained silt or fine-grained sand range, which is always derived from nearby, sandy sources, such as a river terrace, outcropping sandy substratum, dry interfluvies, or even pre-existing sand dunes (Enzel et al., 2010). The source area of this component is local and the transport distance is short, in the range of hundreds of meters or a few kilometers (Vandenberghe, 2013). EM3 and EM2 have a clear inverse relationship (Fig. 5), which implies that they are controlled by the same dynamic mechanism. EM4

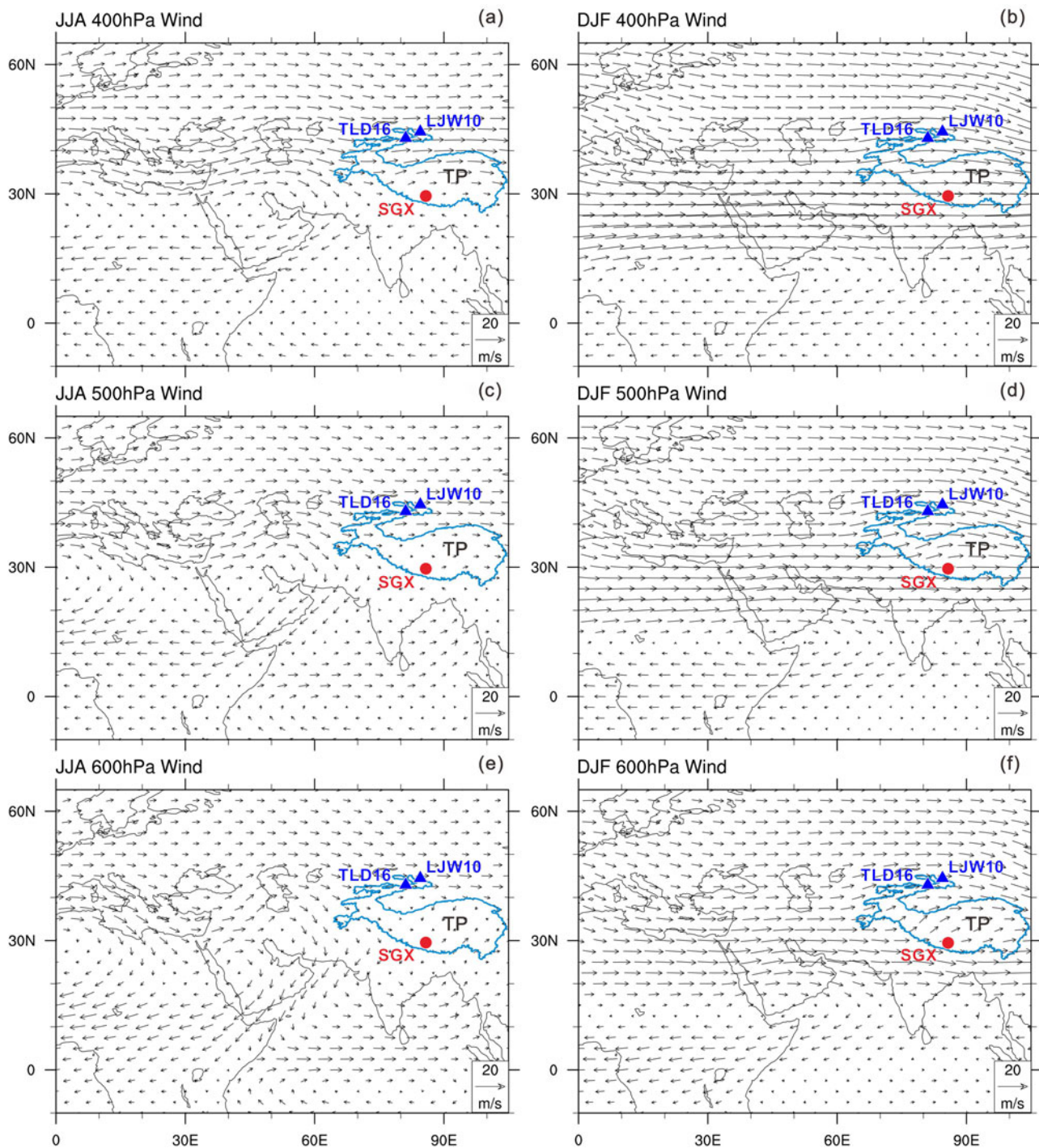


**Figure 6.** Atmospheric circulations over the Tibetan Plateau (TP) and the surrounding regions. Wind circulation at the 400, 500, and 600 hPa levels in (a, c, e) summer (JJA: June, July, and August) and (b, d, f) winter (DJF: December, January and February). Data are from the National Center for Environmental Prediction/National Center for Atmospheric Research.

is the coarsest sediment component, with the modal grain size reaching  $243 \mu\text{m}$ ; it is likely that in the southern Tibetan Plateau this component is transported by dust storms.

#### ***Change in the intensity of the winter mid-latitude Westerlies during the Holocene and its possible driving mechanism***

In the SGX section, low values of EM1 occurred before ca. 6 ka, after which the percentages increased rapidly. This suggests that

weak winter MLW occurred during the Early to Middle Holocene, and stronger winter MLW occurred during the Middle to Late Holocene (Fig. 5). We compared our results with those from loess sections in the Tien Shan Mountains, eastern Central Asia, which are dominated by the MLW at the 400 hPa, 500 hPa, and 600 hPa levels, in winter and summer. The results of grain-size analysis of loess deposits in the northern Tien Shan Mountains indicate weak MLW before 6 ka, but stronger MLW thereafter (Jia et al., 2018). The results of grain-size

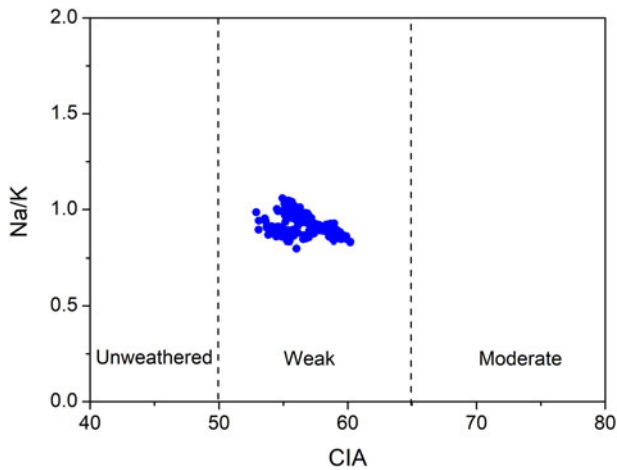


**Figure 7.** Scatter plot of the chemical index of weathering (CIA) versus Na/K of the aeolian sediments of the SGX section. The Na/K data are from Yang *et al.*, 2021.

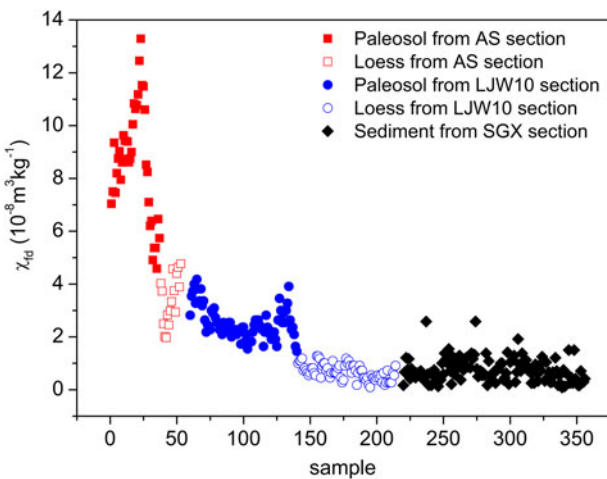


**Figure 8.** Comparison of the frequency-dependent magnetic susceptibility of the SGX section (this study), LJW10 section in the Tien Shan Mountains (Chen *et al.*, 2016), and AS section in the Chinese Loess Plateau (Gao *et al.*, 2019).

analysis of Holocene loess deposits from the Yili valley in eastern Central Asia also suggest that the MLW were weak before 6 ka and stronger thereafter (Wang *et al.*, 2019). The results from eastern Central Asia are therefore very consistent with our results from the southern Tibetan Plateau, which is dominated by the MLW in winter. This consistency has two implications: first, our reconstruction is reliable; and second, the winter MLW made a large contribution to the overall changes in the MLW during the Holocene.

Based on the daily air-surface temperature data from 468 meteorological stations in mainland China for 1960–2013, the variations of the MLW during warm and cold periods in winter were analyzed (Liang *et al.*, 2014). These results from meteorological data indicated that weak MLW occurred during cold periods and stronger MLW occurred during warm periods. This suggests that the variation of the winter MLW is closely linked to temperature, which in turn is closely related to variations in winter insolation in the Northern Hemisphere (Jin *et al.*, 2014). Chen *et al.* (2016) suggested that the winter insolation at mid-latitudes in the Northern Hemisphere increased more rapidly than that at

high latitudes from the early to the late Holocene, resulting in an increased insolation gradient. The insolation gradient between middle and high latitudes can be considered as a temperature gradient, and thus it represents the strength of the MLW (Jin *et al.*, 2014). Therefore, relatively low winter insolation during the Early to Middle Holocene could have resulted in a smaller radiation gradient between middle and high latitudes. A smaller radiation gradient would in turn have led to a decreased temperature gradient, which would have further weakened the winter MLW (Jin *et al.*, 2014; Chen *et al.*, 2016). From the Middle to Late Holocene, the relatively high winter insolation resulted in a larger radiation gradient between middle and high latitudes, which increased the temperature gradient and hence the intensity of the winter MLW.

The intensity of the winter MLW is also closely linked to the strength of the subtropical high, which is dominated by the pressure gradient force between low and high latitudes. The insolation gradient could be considered as a temperature gradient (Jin *et al.*, 2014), and thus as a pressure gradient. Figure 9a shows that the winter insolation gradient between low and high latitudes increased gradually from the Middle to the Late Holocene; therefore, the temperature and pressure gradients between low and high latitudes and the strength of the subtropical high both increased from the Middle to the Late Holocene, causing the winter MLW to gradually intensify. Although we suggest that the variation in Northern Hemisphere winter insolation is the main factor controlling the winter MLW, the influence of Northern Hemisphere ice sheets and atmospheric CO<sub>2</sub> concentration on past variations of the winter MLW cannot be completely excluded, which may also be the reason why the winter MLW (EM1) and the insolation gradient between low and high latitudes are not completely consistent. Therefore, the mechanism responsible for the variation in the winter MLW needs to be further studied in the future.

#### *Influence of the winter mid-latitude Westerlies on regional climate change*

Modern observations reveal that the MLW are the major source of precipitation in arid Central Asia (Karger *et al.*, 2017), and they also influence precipitation in the southern Tibetan Plateau (Tian *et al.*, 2005). The MLW transport water vapor from the water bodies upwind, such as the Mediterranean Sea, Caspian Sea and Black Sea, to regions downwind. Weaker winter MLW occurred during the Early to Middle Holocene (before ca. 6 ka), and stronger winter MLW occurred during the Middle to Late Holocene; therefore, the winter MLW transported more water vapor to the regions downwind during the Middle to Late Holocene compared to the Early to Middle Holocene. Thus, the precipitation in the downwind region during the Middle to Late Holocene was greater than that during the Early to Middle Holocene. Records from loess-paleosol sequences and lake sediments indicate a dry Early to Middle Holocene and a wet Middle to Late Holocene in arid Central Asia (e.g., Wang *et al.*, 2013; Chen *et al.*, 2016; Gao *et al.*, 2019; Fig. 9c–e). This finding is largely consistent with the variation of the winter MLW during the Holocene.

In the southern Tibetan Plateau, due to the influence of the winter MLW, the pattern of moisture variations during the Holocene is not completely consistent with the evolution of Indian summer monsoon. During the Early Holocene, moisture conditions were mainly influenced by the stronger Indian

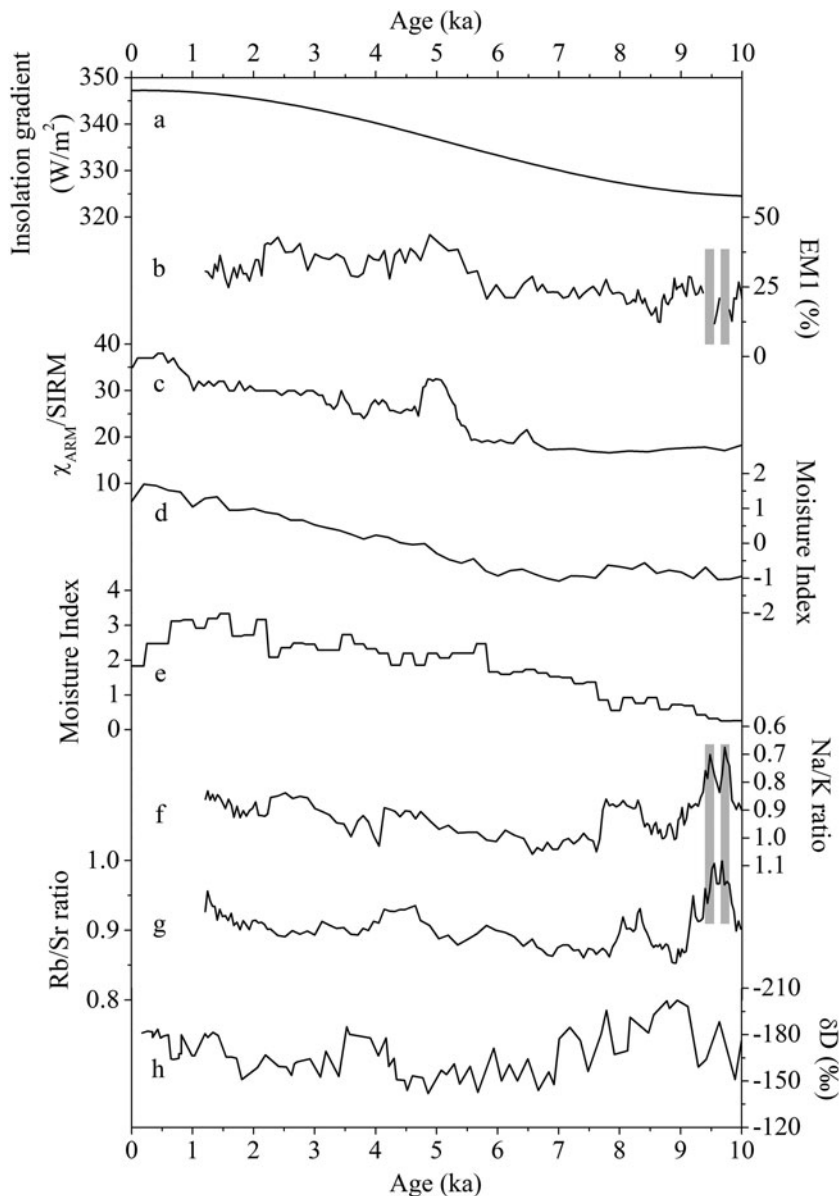


**Figure 9.** (a) Insolation gradient between low and high latitudes (low latitude insolation = average of the insolation at 0°N, 5°N, 10°N, 15°N, and 20°N; high latitude insolation = average of the insolation at 60°N, 65°N, and 70°N). (b) Variations in the winter mid-latitude Westerlies during the Holocene indicated by EMI (this study). (c) Trend of moisture evolution during the Holocene recorded by the  $\chi_{ARM}/SIRM$  record of the LJW10 loess-paleosol section (Chen et al., 2016). (d) Synthesis of records of moisture changes in the arid Central Asia (Gao et al., 2019). (e) Synthesis of records of moisture conditions in the Xinjiang region, China (Wang et al., 2013). (f, g) Changes in moisture conditions indicated by the Na/K and Rb/Sr records from the SGX section in the southern Tibetan Plateau (Yang et al., 2021). (h) Changes in moisture conditions indicated by the  $\delta D$  record from Linggo Co in the central Tibetan Plateau (Hou et al., 2017). The grey bars represent two gravel layers in the SGX section.

summer monsoon and the influence of the weaker winter MLW on moisture supply was negligible. The strong Indian summer monsoon resulted in humid conditions during the Early Holocene. Probably due to the weakening of the Indian summer monsoon and the weaker winter MLW, dry conditions occurred in the study area during the Middle Holocene. From the Middle to the Late Holocene, the water vapor carried by the enhanced MLW compensated for the decreased water vapor supply from the weakened Indian summer monsoon, resulting in an increase in moisture during the Late Holocene (Hou et al., 2017; Chen et al., 2019; Yang et al., 2021).

## CONCLUSIONS

Modern observations of wind circulation suggest that the southern Tibetan Plateau is influenced solely by the MLW in winter and mainly by the Indian summer monsoon in summer. To assess the seasonal variations of the MLW during the Holocene, we

conducted detailed grain-size analyses of a well-dated Holocene aeolian sedimentary sequence from the Yarlung Zangbo River valley in the southern Tibetan Plateau. The results reveal the trend of variation of the winter MLW during the Holocene. Weak winter MLW occurred during the Early to Middle Holocene, and stronger MLW during the Middle to Late Holocene. We suggest that this pattern was closely related to the insolation/temperature/pressure gradient between low and high latitudes in the Northern Hemisphere.

**Supplementary Material.** The supplementary material for this article can be found at <https://doi.org/doi:10.1017/qua.2021.65>

**Acknowledgments.** We thank Dr. Jan Bloemendal for editing the English language. We are grateful to the journal's editors and two reviewers for their valuable comments and suggestions for improving the manuscript.

**Financial Support.** This work was supported by the Second Tibetan Plateau Scientific Expedition and Research Program (STEP) (2019QZKK0602), the Doctoral Research Fund of Lanzhou City University (LZCUBS2019-21), and



the Open Foundation of MOE Key Laboratory of Western China's Environmental System, Lanzhou University, and Fundamental Research Funds for the Central Universities (lzujbky-2019-kb01).

## REFERENCES

- An, C.B., Lu, Y.B., Zhao, J.J., Tao, S.C., Dong, W.M., Li, H., Jin, M., Wang, Z.L., 2012. A high-resolution record of Holocene environmental and climatic changes from Lake Balikun (Xinjiang, China): Implications for central Asia. *The Holocene* **22**, 43–52.
- Chen, F.H., Jia, J., Chen, J.H., Li, G.Q., Zhang, X.J., Xie, H.C., Xia, D.S., Huang, W., An, C.B., 2016. A persistent Holocene wetting trend in arid central Asia, with wettest conditions in the Late Holocene, revealed by multi-proxy analyses of loess-paleosol sequences in Xinjiang, China. *Quaternary Science Reviews* **146**, 134–146.
- Chen, F.H., Chen, J.H., Huang, W., Chen, S.Q., Huang, X.Z., Jin, L.Y., Jia, J., et al., 2019. Westerlies Asia and monsoonal Asia: spatiotemporal differences in climate change and possible mechanisms on decadal to sub-orbital timescales. *Earth-Science Reviews* **192**, 337–354.
- Duan, F.T., An, C.B., Wang, W., Herzschuh, U., Zhang, M., Zhang, H.X., Liu, Y., Zhao, Y.T., Li, G.Q., 2020. Dating of a late Quaternary loess section from the northern slope of the Tianshan Mountains (Xinjiang, China) and its paleoenvironmental significance. *Quaternary International* **544**, 104–122.
- Enzel, Y., Amit, R., Crouvi, O., Porat, N., 2010. Abrasion-derived sediments under intensified winds at the latest Pleistocene leading edge of the advancing Sinai-Negev erg. *Quaternary Research* **74**, 121–131.
- Fleitmann, D., Burns, S.J., Mangini, A., Mudelsee, M., Kramers, J., Villa, I., Neff, U., et al., 2007. Holocene ITCZ and Indian monsoon dynamics recorded in stalagmites from Oman and Yemen (Socotra). *Quaternary Science Reviews* **26**, 170–188.
- Gao, F.Y., Jia, J., Xia, D.S., Lu, C.C., Lu, H., Wang, Y.J., Liu, H., Ma, Y.P., Li, K.M., 2019. Asynchronous Holocene Climate Optimum across mid-latitude Asia. *Palaeogeography, Palaeoclimatology, Palaeoecology* **518**, 206–214.
- Hou, J.Z., D'Andrea, W.J., Wang, M.D., He, Y., Liang, J., 2017. Influence of the Indian monsoon and the subtropical jet on climate change on the Tibetan Plateau since the late Pleistocene. *Quaternary Science Reviews* **163**, 84–94.
- Jia, J., Liu, H., Gao, F.Y., Xia, D.S., 2018. Variations in the Westerlies in Central Asia since 16 ka recorded by a loess section from the Tianshan Mountains. *Palaeogeography, Palaeoclimatology, Palaeoecology* **504**, 156–161.
- Jin, L.Y., Schneider, B., Park, W., Latif, M., Khon, V., Zhang, X.J., 2014. The spatial-temporal patterns of Asian summer monsoon precipitation in response to Holocene insolation change: a model-data synthesis. *Quaternary Science Reviews* **85**, 47–62.
- Karger, D.N., Conrad, O., Bohner, J., Kawohl, T., Kreft, H., Soriauza, R.W., Zimmermann, N.E., Linder, H.P., Kessler, M., 2017. Climatologies at high resolution for the Earth's land surface areas. *Scientific Data* **4**, 170122. <https://doi.org/10.1038/sdata.2017.122>.
- Kumar, O., Ramanathan, A.L., Bakke, J., Kotlia, B.S., Shrivastava, J.P., Kumar, P., Sharma, R., Kumar, P., 2021. Role of Indian Summer Monsoon and Westerlies on glacier variability in the Himalaya and East Africa during Late Quaternary: Review and new data. *Earth-Science Reviews* **212**, 103431. <https://doi.org/10.1016/j.earscirev.2020.103431>.
- Liang, S.J., Ding, Y.H., Zhao, N., Sun, Y., 2014. Analysis of the interdecadal changes of the wintertime surface air temperature over mainland China and regional atmospheric circulation characteristics during 1960–2013. *Chinese Journal of Atmospheric Sciences* **38**, 974–992. [in Chinese]
- Ling, Z.Y., Jin, J.H., Wu, D., Liu, X.J., Xia, D.S., Chen, F.H., 2019. Aeolian sediments and their paleoenvironmental implication in the Yarlung Zangbo catchment (southern Tibet, China) since MIS3. *Acta Geographica Sinica* **74**, 2385–2400. [in Chinese]
- Ling, Z.Y., Yang, X.Y., Wang, Y.X., Wang, Y.R., Jin, J.H., Zhang, D.J., Chen, F.H., 2020. OSL chronology of the Liena archeological site in the Yarlung Tsangpo valley throws new light on human occupation of the Tibetan Plateau. *The Holocene* **30**, 1043–1052.
- Long, H., Shen, J., Chen, J., Tsukamoto, S., Yang, L.H., Cheng, H.Y., Frechen, M., 2017. Holocene moisture variations over the arid central Asia revealed by a comprehensive sand-dune record from the central Tian Shan, NW China. *Quaternary Science Reviews* **174**, 13–32.
- Lu, H.Y., An, Z.S., 1998. Pretreatment methods in loess-paleosol granulometry. *Chinese Science Bulletin* **43**, 237–240.
- McLennan S.M., 1993. Weathering and global denudation. *The Journal of Geology* **101**, 295–303.
- Pye, K., 1987. *Aeolian Dust and Dust Deposits*. Academic Press, London.
- Pye, K., 1995. The nature, origin and accumulation of loess. *Quaternary Science Reviews* **14**, 653–667.
- Schiemann R, Lüthi D, Schär C., 2009. Seasonality and interannual variability of the Westerly Jet in the Tibetan Plateau region. *Journal of Climate* **22**, 2940–2957.
- Shen, W.S., Li, H.D., Sun, M., Jiang, J., 2012. Dynamics of aeolian sandy land in the Yarlung Zangbo River basin of Tibet, China from 1975 to 2008. *Global and Planetary Change* **86–87**, 37–44.
- Song, Y.G., Yang, S.L., Nie, J.S., Zan, J.B., Song, C.H., 2021. Preface (volume I): Quaternary paleoenvironmental changes in Central Asia. *Palaeogeography, Palaeoclimatology, Palaeoecology* **568**, 110319. <https://doi.org/10.1016/j.palaeo.2021.110319>.
- Sun, J.M., 2002. Source regions and formation of the loess sediments on the high mountain regions of northwestern China. *Quaternary Research* **58**, 341–351.
- Sun, Z., Yuan, K., Hou, X.H., Ji, K.J., Li, C.G., Wang, M.D., Hou, J.Z., 2020. Centennial-scale interplay between the Indian Summer Monsoon and the Westerlies revealed from Ngamring Co, southern Tibetan Plateau. *The Holocene* **30**, 1163–1173.
- Tian, L.D., Yao, T.D., White, J.W., Yu, W.S., Wang, N.L., 2005. Westerly moisture transport to the middle of Himalayas revealed from the high deuterium excess. *Chinese Science Bulletin* **50**, 1026–1031.
- Vandenbergh J., 2013. Grain size of fine-grained windblown sediment: a powerful proxy for process identification. *Earth-Science Reviews* **121**, 18–30.
- Wang, L.B., Jia, J., Zhao, H., Liu, H., Duan, Y.W., Xie, H.C., Zhang, D.D., Chen, F.H., 2019. Optical dating of Holocene paleosol development and climate changes in the Yili Basin, arid central Asia. *The Holocene* **29**, 1068–1077.
- Wang, W., Feng, Z. D., Ran, M., Zhang, C. J., 2013. Holocene climate and vegetation changes inferred from pollen records of Lake Aibi, northern Xinjiang, China: A potential contribution to understanding of Holocene climate pattern in East-central Asia. *Quaternary International* **311**, 54–62.
- Wang, Y., Cheng, H., Edwards, R L., He, Y.Q., Kong, X.G., An, Z.S., Wu, J.Y., Kelly, M.J., Dykoski, C.A., Li, X.D., 2005. The Holocene Asian Monsoon: links to solar changes and North Atlantic climate. *Science* **308**, 854–857.
- Yang, J.H., Xia, D.S., Gao, F.Y., Wang, S.Y., Chen, Z.X., Jia, J., Yang, S.L., Ling, Z.Y., 2020a. Aeolian deposits in the Yarlung Zangbo River basin, southern Tibetan Plateau: A brief review. *Advances in Earth Science* **35**, 863–877. [in Chinese]
- Yang, J.H., Xia, D.S., Wang, S.Y., Tian, W.D., Ma, X.Y., Chen, Z.X., Gao, F.Y., Ling, Z.Y., Dong, Z.B., 2020b. Near-surface wind environment in the Yarlung Zangbo River basin, southern Tibetan Plateau. *Journal of Arid Land* **12**, 917–936.
- Yang, J.H., Xia, D.S., Gao, F.Y., Wang, S.Y., Li, D.X., Fan, Y.J., Chen, Z.X., et al., 2021. Holocene moisture evolution and its response to atmospheric circulation recorded by aeolian deposits in the southern Tibetan Plateau. *Quaternary Science Reviews* **270**, 107169. <https://doi.org/10.1016/j.quas-cirev.2021.107169>.